

H. Narayanan · E. M. Arruda · K. Grosh · K. Garikipati

# Recent advances in the mathematics and physics of biological growth models

Received: date / Accepted: date

**Abstract** In this paper, we address some modelling issues related to biological growth. Our treatment is based on a recently-proposed, general formulation for growth within the context of mixture theory (Journal of the Mechanics and Physics of Solids, **52**, 2004, 1595–1625). We aim to enhance this treatment by making it more appropriate for the biophysics of growth in soft tissue, specifically tendon. This involves several modifications to the mathematical formulation to represent the reactions, transport and mechanics, and their interactions. We also reformulate the governing differential equations for reaction-transport to represent the incompressibility constraint on the fluid phase of the tissue. This revision enables a straightforward implementation of numerical stabilisation for the hyperbolic, or advection-dominated, limit. A finite element implementation employing an operator splitting scheme is used to solve the coupled, non-linear partial differential equations that arise from the theory. Motivated by our experimental model, an *in vitro* scaffold-free engineered tendon formed by self-assembly of tendon fibroblasts (Calve et al., 2004), we solve several numerical examples demonstrating biophysical aspects of tissue growth, and the improved numerical performance of the models.

**Keywords** Soft Tissue · Porous Media · Enzyme Kinetics · Advection-Diffusion · Incompressibility · Stabilisation

## 1 Introduction

*Growth* involves the addition or depletion of mass in biological tissue. In biological systems, growth occurs in combination with *remodelling*, which is a change in microstructure, and possibly with *morphogenesis*, which is a change

in form in the embryonic state. The physics of these processes are quite distinct, and for modelling purposes can, and must, be separated. Our previous work (Garikipati et al., 2004), upon which we now seek to build, drew in some measure from Cowin and Hegedus (1976); Epstein and Maugin (2000), and Taber and Humphrey (2001), and was focused upon a comprehensive account of the coupling between transport and mechanics. The origins of this coupling were traced to the balance equations, kinematics and constitutive relations. A major contribution of that work was the identification and discussion of several driving forces for transport that are thermodynamically-consistent, in the sense that specification of these relations does not violate the Clausius-Duhem dissipation inequality. Now, we seek to restrict the range of physically-admissible models in order to gain greater physiological relevance for modelling growth in soft biological tissue. The advection-diffusion equations for mass transport require numerical stabilisation in the advection-dominated regime (the hyperbolic limit). We draw upon the enforcement of the incompressibility limit for the fluid phase to facilitate this development. Below, we briefly introduce each aspect that we have considered, but postpone details until relevant sections in the paper.

- For a tissue undergoing finite strains, the transport equations can be formulated, mathematically, in terms of concentrations with respect to either the reference or current (deformed) configuration. However, the physics of fluid-tissue interactions and the imposition of relevant boundary conditions is best understood and represented in the current configuration.
- The state of saturation is crucial in determining whether the tissue swells or shrinks with infusion/expulsion of fluid. This aspect has been introduced into the formulation.
- The fluid phase, whether slightly compressible or incompressible, can develop compressive stress without bound. However, it can develop at most a small tensile stress (Brennen, 1995), having implications for the stiffness of the tissue in tension as against compression. Though this also has implications for void formation through cavi-

H. Narayanan · E. M. Arruda · K. Grosh · *Correspondence to:* K. Garikipati  
 Department of Mechanical Engineering, University of Michigan,  
 Ann Arbor, Michigan 48109–2125, USA  
 Tel.: +1-734-936-0414, Fax: +1-734-647-9379  
 E-mail: krishna@umich.edu

tation, the ambient pressure in the tissue under normal physiological conditions ensures that this manifests itself only as a reduction in compressive pressure.

- When modelling transport, it is common to assume Fickian diffusion (Kuhl and Steinmann, 2003). This implies the existence of a mixing entropy due to the configurations available to molecules of the diffusing species at fixed values of the macroscopic concentration. The state of fluid saturation directly influences its mixing entropy.
- If fluid saturation is maintained, void formation in the pores is disallowed even under an increase in the pores' volume. This has implications for the fluid exchanges between a deforming tissue and a fluid bath with which it is in contact.
- Recognising the incompressibility of the fluid phase, it is common to treat soft biological tissue as either incompressible or nearly-incompressible (Fung, 1993). At the scale of the pores (the microscopic scale in this case), however, a distinction exists in that the fluid is exactly (or nearly) incompressible, while the porous solid network is not obviously incompressible.
- In Garikipati et al. (2004), the acceleration of the solid phase was included as a driving force in the constitutive relation for the flux of other phases. However, acceleration is not frame-invariant and its use in constitutive relations is inappropriate.
- Chemical solutes in the extra-cellular fluid are advected by the fluid velocity and additionally undergo transport under a chemical potential gradient relative to the fluid. In the hyperbolic limit, where advection dominates, spatial instabilities emerge in numerical solutions of these transport equations (Brooks and Hughes, 1982; Hughes et 1987). Numerical stabilisation of the equations is intimately tied to the mathematical representation of fluid incompressibility.

These issues are treated in detail in relevant sections of the paper, which is laid out as follows: Balance equations and kinematics are discussed in Section 2, constitutive relations for reactions, transport and mechanics in Section 3, and numerical examples are presented in Section 4. Conclusions are drawn in Section 5.

## 2 Balance equations and kinematics of growth

In this section, the coupled, continuum balance equations governing the behaviour of growing tissue are summarised and specialised as outlined in Section 1. For detailed continuum mechanical arguments underlying the equations, the interested reader is directed to Garikipati et al. (2004).

The tissue of interest is an open subset of  $\mathbb{R}^3$  with a piecewise smooth boundary. At a reference placement of the tissue,  $\Omega_0$ , points in the tissue are identified by their reference positions,  $X \in \Omega_0$ . The motion of the tissue is a sufficiently smooth bijective map  $\varphi : \overline{\Omega}_0 \times [0, T] \rightarrow \mathbb{R}^3$ , where  $\overline{\Omega}_0 := \Omega_0 \cup \partial\Omega_0$ ;  $\partial\Omega_0$  being the boundary of  $\Omega_0$ . At a typical

time  $t \in [0, T]$ ,  $\varphi(X, t)$  maps a point  $X$  to its current position,  $x$ . In its current configuration, the tissue occupies a region  $\Omega_t = \varphi_t(\Omega_0)$ . These details are depicted in Figure 1. The deformation gradient  $F := \partial\varphi/\partial X$  is the tangent map of  $\varphi$ .

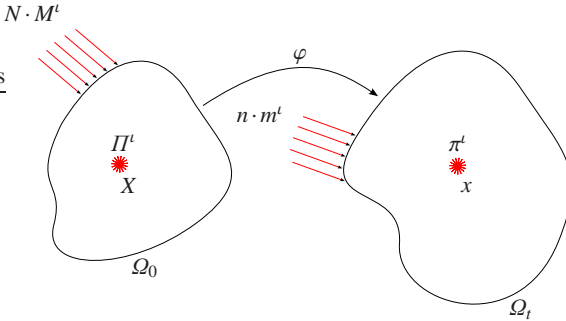


**Fig. 1** The tissue as a continuous medium with growing and diffusing species.

The tissue consists of numerous species, of which the following groupings are of importance for the models: A solid species, consisting of solid *collagen fibrils* and *cells*,<sup>1</sup> denoted by  $c$ , an extra-cellular *fluid* species denoted by  $f$  and consisting primarily of water, and *solute* species, consisting of precursors to reactions, byproducts, nutrients, and other regulatory chemicals. A generic solute will be denoted by  $s$ . In what follows, an arbitrary species will be denoted by  $\iota$ , where  $\iota = c, f, s$ .

The fundamental quantities of interest are mass concentrations,  $\rho_0^\iota(X, t)$ . These are the masses of each species per unit system volume in  $\Omega_0$ . Formally, these quantities can also be thought of in terms of the maps  $\rho_0^\iota : \overline{\Omega}_0 \times [0, T] \rightarrow \mathbb{R}$ , upon which the formulation imposes some smoothness requirements. By definition, the total *material density* of the tissue at a point is a sum of these concentrations over all species  $\sum_\iota \rho_0^\iota = \rho_0$ . Other than the solid species,  $c$ , all phases have mass fluxes,  $M^\iota$ . These are mass flow rates per unit cross-sectional area in the reference configuration *defined relative to the solid phase*. The species have mass sources (or sinks),  $\Pi^\iota$ .

### 2.1 Balance of mass for an open system

As a result of mass transport (via the flux terms) and interconversion of species (via the source/sink terms) introduced above, the concentrations,  $\rho_0^\iota$ , change with time. In local form, the balance of mass for an arbitrary species in the reference configuration is

$$\frac{\partial \rho_0^\iota}{\partial t} = \Pi^\iota - \text{DIV}[M^\iota], \forall \iota, \quad (1)$$

<sup>1</sup> At this point, we do not distinguish the solid species further. This is a good approximation to the physiological setting for tendons, which are relatively acellular and whose dry mass consists of up to 75% collagen (Nordin et al., 2001).

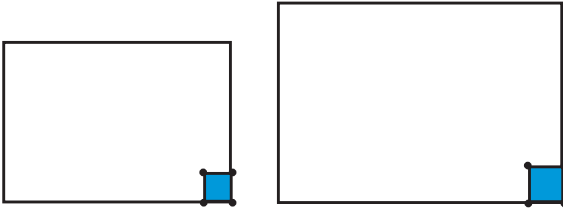


**Fig. 2** If the pore structure at the boundary deforms with the tissue and this boundary is in contact with a fluid bath, the fluid concentration with respect to the current configuration, i.e.,  $\rho^f$ , remains constant.

recalling that, in particular,  $M^c = \mathbf{0}$ . Here,  $\text{DIV}[\bullet]$  is the divergence operator in the reference configuration. The functional forms of  $\Pi^\iota$  are abstractions of the underlying biochemistry, physiologically relevant examples of which are discussed in Section 3.4, and the fluxes,  $M^\iota$ , are determined from the thermodynamically-motivated constitutive relations described in Section 3.3.

The behaviour of the entire system can be determined by summing Equation (1) over all species  $\iota$ . Additionally, sources and sinks satisfy the relation

$$\sum_\iota \Pi^\iota = 0, \quad (2)$$

which is consistent (Garikipati et al., 2004) with the Law of Mass Action for reaction rates and with mixture theory (Truesdell and Noll, 1965).

### 2.1.1 The role of mass balance in the current configuration

Although the initial-boundary-value problem of mass transport is consistently posed in the reference configuration, it is important to note that as soft tissues deform, the current configuration,  $\Omega_t$ , and its boundary,  $\partial\Omega_t$ , change in time. We assume that the species undergoing transport deforms with the solid phase. Therefore, the deformation gradient,  $F$ , is common to  $c$ ,  $f$ , and  $s$ . Specifically, the pore structure deforms with the tissue. Therefore, at the boundary the fluid concentration with respect to  $\Omega_t$  remains constant if the boundary is in contact with a fluid bath. Accordingly, this is the appropriate Dirichlet boundary condition to impose under normal physiological conditions. This is shown in an idealised manner in Figure 2.

In the interest of applying boundary conditions (either specification of species flux or concentration) that are physically meaningful, we use the local form of the balance of mass in the current configuration,

$$\frac{d\rho^\iota}{dt} = \pi^\iota - \text{div}[m^\iota] - \rho^\iota \text{div}[v], \quad \forall \iota, \quad (3)$$

where  $\rho^\iota(x, t)$ ,  $\pi^\iota(x, t)$ , and  $m^\iota(x, t)$  are the current mass concentration, source and mass flux of species  $\iota$  respectively and  $v(x, t)$  is the velocity of the solid phase. They are related to corresponding reference quantities as  $\rho^\iota = (\det(F))^{-1} \rho_0^\iota$ ,

$\pi^\iota = (\det(F))^{-1} \Pi^\iota$  and  $m^\iota = (\det(F))^{-1} F M^\iota$ . The spatial divergence operator is  $\text{div}[\bullet]$ , and the left hand-side in Equation (3) is the material time derivative, that may be written explicitly as  $\frac{\partial}{\partial t}|_X$ , implying that the reference position is held fixed.

### 2.2 The kinematics of growth (changes in mass concentration)

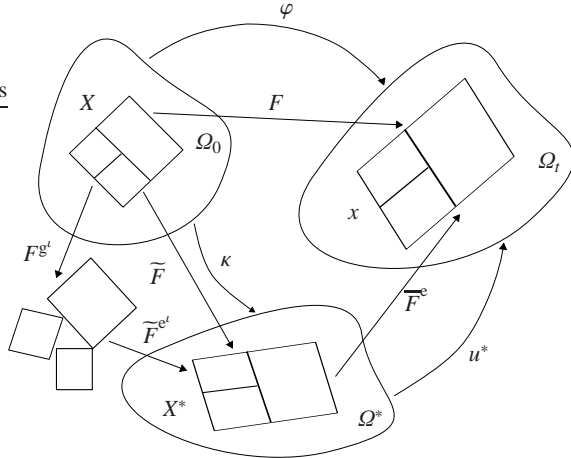


**Fig. 3** The kinematics of growth.

Local volumetric changes are associated with changes in the concentrations of species. The material of the species swells with an increase in concentration (mass of the species per unit system volume), and shrinks as its concentration decreases. This leads to the notion of a *growth deformation gradient*. One aspect of the coupling between mass transport and mechanics stems from this phenomenon. In the setting of finite strain kinematics, the total deformation gradient is decomposed into the growth deformation gradient, a *geometrically-necessitated elastic deformation* accompanying growth, and an *additional elastic deformation due to external stress*. This split is analogous to the classical decomposition of multiplicative plasticity (Lee, 1969) and is similar to the approach followed in existing literature on biological growth (see, for e.g., Taber and Humphrey (2001); Ambrosi and Mollica (2002)).

The split itself is visualised in Figure 3. Assuming that the volume changes associated with growth described above are isotropic, a simple form for the growth deformation gradient tensor is

$$F^{g^t} = \left( \frac{\rho_0^\iota}{\rho_{0_{\text{ini}}}^\iota} \right)^{\frac{1}{3}} \mathbf{1}, \quad (4)$$

where  $\rho_{0_{\text{ini}}}^\iota(X)$  is the reference state at the initial time, and  $\mathbf{1}$  is the second-order isotropic tensor. In this state,  $F = F^{g^t}$ , the species would be stress free in the absence of a deformation.

The kinematics being local, the action of  $F^{g^t}$  alone can result in incompatibility, which is eliminated by the geometrically-necessary elastic deformation  $\tilde{F}^{e^t}$ . Thus, the total deformation gradient is  $F = \bar{F}^e \tilde{F}^{e^t} F^{g^t}$ , where  $\bar{F}^e$  arises from the external stress, and internal stresses in the tissue arise due to the compatibility restoring tensor  $\tilde{F}^{e^t}$ .

### 2.2.1 Saturation and tissue swelling

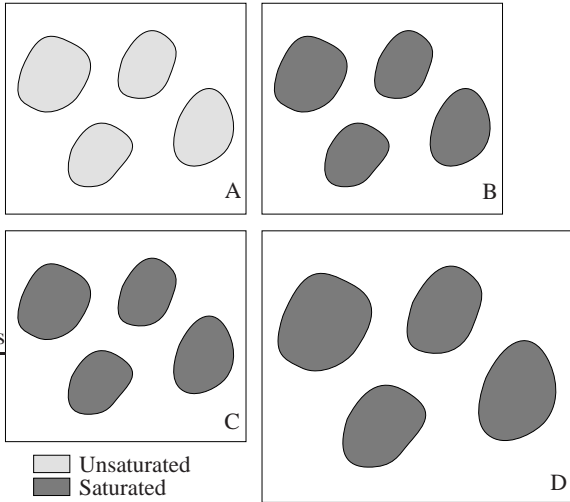


**Fig. 4** Initially unsaturated tissue (A) allows influx of fluid without swelling until it is completely saturated (B). Initially saturated tissue (C) swells with influx of fluid (D).

Upon closer examination of the solid phase of the tissue as a porous medium, it is observed that its degree of saturation plays a fundamental role in determining whether the tissue responds by swelling or shrinking to an infusion or expulsion of fluid. In particular, the isotropic swelling law defined by Equation (4) has to be generalised to treat the case in which the solid phase is not saturated by fluid.

Figure 4 schematically depicts two potential scenarios. If the tissue is initially unsaturated (as in A), this corresponds to the fact that, on a microscopic scale, it still contains unfilled voids. It is thus capable of allowing an influx of fluid, which tends to increase its degree of saturation (to reach B), but does not cause the tissue to swell, as there is free volume for incoming fluid to occupy. However, if the tissue is initially saturated (as in C), an increase in the amount of fluid will result in swelling (as depicted in D), as there is no free volume for the entering fluid to occupy. It is this second case that is modelled by (4).

The isotropic swelling law can be extended to the unsaturated case by introducing a degree of saturation arising in a natural fashion from the current concentrations,  $\rho^t$ . These quantities can also be thought of as the product of the intrinsic density of the species,  $\tilde{\rho}^t$ , and the corresponding volume fraction,  $\tilde{v}^t$ , in the current configuration. Upon solution of the

mass balance equation (3) for  $\rho^t$ , the species volume fractions,  $\tilde{v}^t$ , can be computed since the intrinsic densities are known material properties. The sum of these volume fractions is our required measure of saturation, and clearly cannot exceed unity in the current configuration. We thus proceed to redefine the growth deformation gradient tensor as follows:

$$F^{g^t} = \begin{cases} \mathbf{1}, & \sum_i \tilde{v}^t < 1 \\ \left( \frac{\rho_0^t}{\rho_{0,ini}^t} \right)^{\frac{1}{3}} \mathbf{1}, & \text{otherwise.} \end{cases} \quad (5)$$

However, it is important to note that under normal physiological conditions, soft tissues are fully saturated by the fluid and Equation (4) is appropriate.

### 2.3 Balance of momenta

In soft tissues, the species production rate and flux that appear on the right hand-side in Equation (1), are strongly dependent on the local state of stress. To correctly model this coupling, the balance of linear momentum should be solved to determine the local state of strain and stress.

The deformation of the tissue is characterised by the map  $\varphi(X, t)$ . Recognising that, in tendons, the solid collagen fibrils and fibroblasts do not undergo mass transport,<sup>2</sup> the material velocity of this species,  $V = \partial\varphi/\partial t$ , is used as the primitive variable for mechanics. The motion of each remaining species is split into a deformation along with the solid species, and mass transport relative to it. To this end, it is useful to define the material velocity of a species  $\iota$  relative to the solid skeleton as:  $V^\iota = (1/\rho_0^\iota) F M^\iota$ . Thus, the total material velocity of a species  $\iota$  is  $V + V^\iota$ .

The total first Piola-Kirchhoff stress tensor,  $P$ , is the sum of the partial stresses  $P^\iota$  (borne by a species  $\iota$ ) over all the species present.<sup>3</sup> With the introduction of these quantities, the balance of linear momentum in local form for a species  $\iota$  in  $\Omega_0$  is

$$\rho_0^\iota \frac{\partial}{\partial t} (V + V^\iota) = \rho_0^\iota (g + q^\iota) + \text{DIV}[P^\iota] - (\text{GRAD}[V + V^\iota]) M^\iota, \quad (6)$$

where  $g$  is the body force per unit mass, and  $q^\iota$  is an interaction term denoting the force per unit mass exerted upon  $\iota$  by all other species present. The final term with the (reference) gradient denotes the contribution of the flux to the balance of momentum. In practise, the relative magnitude of the fluid mobility (and hence flux) is small, so the final term on the right hand side of Equation (6) is negligible, resulting in a

<sup>2</sup> Currently, we do not consider certain physiological processes, such as the migration of fibroblasts within the extra-cellular matrix during wound healing, which may otherwise be modelled as mass transport.

<sup>3</sup> Solutes such as amino acids, nutrients and regulators are in low concentrations, and do not bear appreciable stress.

more classical form of the balance of momentum. Furthermore, in the absence of significant acceleration of the tissue during growth, the left hand-side can also be neglected, reducing (6) to the quasi-static balance of linear momentum.

The balance of momentum of the entire tissue is obtained by summing Equation (6) over all  $\iota$ . Additionally, recognising that the rate of change of momentum of the entire tissue is affected only by external agents and is independent of internal interactions, the following relation arises.

$$\sum_{\iota} (\rho_0^{\iota} q^{\iota} + \Pi^{\iota} V^{\iota}) = 0. \quad (7)$$

This is also consistent with Classical Mixture Theory (Truesdell 1965). See Garikipati et al. (2004) for further details on balance of linear momentum, and the formulation of balance of angular momentum. We only note here that the latter principle leads to a symmetric partial Cauchy stress,  $\sigma^{\iota}$  for each species in contrast with the unsymmetric Cauchy stress of Epstein and Maugin (2000).

### 3 Constitutive framework and specific models

As is customary in field theories of continuum physics, the Clausius-Duhem inequality is obtained by multiplying the entropy inequality (the Second Law of Thermodynamics) by the temperature field,  $\theta$ , and subtracting it from the balance of energy (the First Law of Thermodynamics). We assume the Helmholtz free energy per unit mass of species  $\iota$  to be of a sufficiently general form:  $\psi^{\iota} = \hat{\psi}^{\iota}(F^{\iota}, \theta, \rho_0^{\iota})$ . Substituting this in the Clausius-Duhem inequality results in a form of this inequality that the specified constitutive relations *must not* violate. Only the valid constitutive laws relevant to the examples that follow are listed here. For details, see Garikipati et al. (2004).

#### 3.1 An anisotropic network model based on entropic elasticity

The partial first Piola-Kirchhoff stress of collagen, modelled as a hyperelastic material, is  $P^c = \rho_0^c \partial \psi^c / \partial F^c$ . Recall that  $F^c = F F^{g^c - 1}$  is the elastic deformation gradient, and  $F^{g^c}$  is the growth deformation gradient, of collagen. Following Equation (4), if we were considering unidirectional growth of collagen along a unit vector  $e$ , we would have  $F^{g^c} = \frac{\rho_0^c}{\rho_{0_{ini}}^c} e \otimes e$ , with  $\rho_{0_{ini}}^c$  denoting the initial concentration of collagen at the point.

The mechanical response of tendons in tension is determined primarily by their dominant structural component: highly oriented fibrils of collagen. In our preliminary formulation, the strain energy density for collagen has been obtained from hierarchical multi-scale considerations based upon an entropic elasticity-based worm-like chain (WLC) model (Kratky and Porod, 1949). The WLC model has been

widely used for long chain single molecules, most prominently for DNA (Marko and Siggia, 1995; Rief et al., 1997; Bustamante et al., 2003), and recently for the collagen monomer (Sun et al., 2002). The central parameters of this model are the chain's contour length,  $L$ , and persistence length,  $A$ . The latter is a measure of its stiffness and given by  $A = \chi/k\theta$ , where  $\chi$  is the bending rigidity,  $k$  is Boltzmann's constant and  $\theta$  is the temperature. See Landau and Lifshitz (1951) for general formulation of statistical mechanics models of long chain molecules.

To model a collagen network structure, the WLC model has been embedded as a single constituent chain of an eight-chain model (Bischoff et al., 2002a,b), depicted in Figure 5. Homogenisation via averaging then leads to a continuum Helmholtz free energy function,  $\psi_F^c$ :<sup>4</sup>

$$\begin{aligned} \rho_0^c \psi_F^c(F^c) &= \frac{Nk\theta}{4A} \left( \frac{r^2}{2L} + \frac{L}{4(1-r/L)} - \frac{r}{4} \right) \\ &+ \frac{\gamma}{\beta} (J^{e^{c-2\beta}} - 1) + \gamma \mathbf{1} : (C^c - \mathbf{1}) \\ &- \frac{Nk\theta}{4\sqrt{2L/A}} \left( \sqrt{\frac{2A}{L}} + \frac{1}{4(1-\sqrt{2A/L})} - \frac{1}{4} \right) Z, \\ Z &= \log \left( \lambda_1^{e^a} \lambda_2^{e^b} \lambda_3^{e^c} \right). \end{aligned} \quad (8)$$

Here,  $N$  is the density of chains, and  $a, b$  and  $c$  are lengths of the unit cell sides aligned with the principal stretch directions. The material model is isotropic only if  $a = b = c$ .

The elastic stretches along the unit cell axes are respectively denoted by  $\lambda_1^e, \lambda_2^e$  and  $\lambda_3^e$ ,  $C^c = F^c F^{c^T}$  is the elastic right Cauchy-Green tensor of collagen. The factors  $\gamma$  and  $\beta$  control the bulk compressibility of the model. The end to end chain length is given by  $r = \frac{1}{2} \sqrt{a^2 \lambda_1^{e^2} + b^2 \lambda_2^{e^2} + c^2 \lambda_3^{e^2}}$ , where  $\lambda_I^e = \sqrt{N_I \cdot C^c N_I}$ , and  $N_I, I = 1, 2, 3$  are the unit vectors along the three unit cell axes, respectively. In our numerical simulations that appear below in Section 4, the numerical values used for the parameters introduced in (8) are based on those in Kuhl et al. (2005).

#### 3.2 A nearly incompressible ideal fluid

In this preliminary work, the fluid phase is treated as nearly incompressible and ideal, i.e., inviscid. The partial Cauchy stress in the fluid is

$$\sigma^f = \det(F^f)^{-1} P^f F^{f^T} = h(\rho^f) \mathbf{1}, \quad (9)$$

where a large value of  $h'(\rho^f)$  ensures near-incompressibility.

<sup>4</sup> Under the isothermal conditions assumed here, the only variation in  $\psi^c$  is from the strain energy. Accordingly, we have the parametrisation  $\psi_F^c = \psi_F^c(F^c)$ .

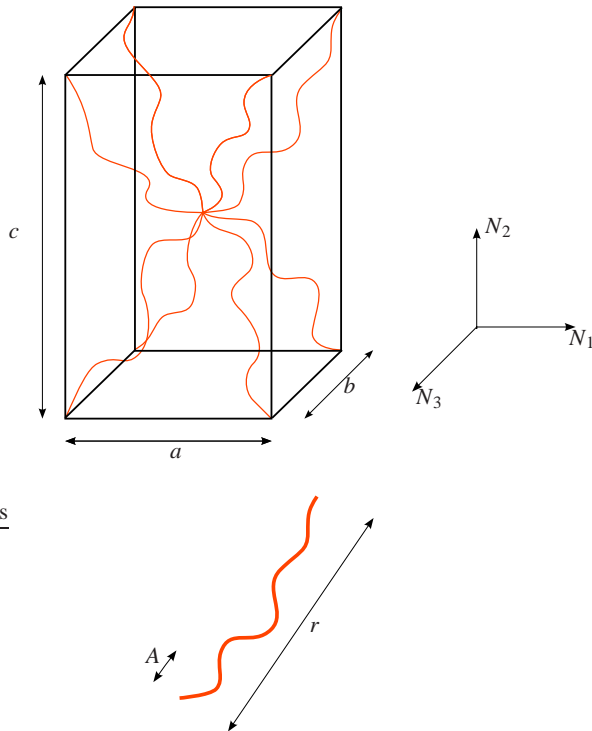


**Fig. 5** The eight-chain model incorporating worm-like chains.

### 3.2.1 Response of the fluid in tension; cavitation

The response of the ideal fluid, as defined by Equation (9), does not explicitly distinguish between the cases where the fluid is subjected to tension or compression, i.e., whether  $\det(F^e) \gtrless 1$ . Being (nearly) incompressible, the fluid can develop compressive stresses without bound—a case that is modelled accurately. However, the fluid can develop at most a small tensile stress (Brennen, 1995),<sup>5</sup> and the bulk of the tensile stiffness arises from the collagen phase. This is not accurately represented by (9), which models a symmetric response in tension and compression.

Here, we preclude all tensile load carrying by the fluid by limiting  $\det(F^e) \leq 1$ . For consistency, we first introduce an additional component to the mixture, a *void* species,  $v$ . Denoting its deformation gradient by  $F^v$ , we now only require

$$F^e F^v = F, \quad (10)$$

where  $F$  is the pointwise homogeneous deformation gradient.

We restrict the formulation to include only saturated reference configurations at  $t = 0$ . At times  $t \neq 0$  if  $\det(F) < 1$ , we set  $F^v = \mathbf{1}$ , denoting no voids and a persistence of saturation. Otherwise, we set  $\det(F^e) = 1$  and allow the pores

<sup>5</sup> Where, we are referring to the fluid being subject to net tension, not a reduction in fluid compressive stress from reference ambient pressure.

to evacuate, (i.e. allow  $\det(F^v) > 1$ ), giving us an additional measure of the unsaturation in the system.

### 3.3 Constitutive relations for fluxes

From Garikipati et al. (2004), the constitutive relation for the flux of extra-cellular fluid relative to collagen in the reference configuration takes the following form,

$$M^f = D^f (\rho_0^f F^T g + F^T \text{DIV} [P^f] - \text{GRAD} [e^f - \theta \eta^f]), \quad (11)$$

where  $D^f$  is the positive semi-definite mobility of the fluid and isothermal conditions are assumed to approximate the physiological ones. Experimentally determined transport coefficients (e.g. for mouse tail skin (Swartz et al., 1999) and rabbit Achilles tendons (Han et al., 2000)) are used for the fluid mobility values. The terms in the parenthesis on the right hand-side of Equation (11) sum to give the total driving force for transport. The first term is the contribution due to gravitational acceleration. In order to maintain physiological relevance, this term has been neglected in the following treatment. The second term arises from stress divergence; for an ideal fluid, it reduces to a pressure gradient, thereby specifying that the fluid moves down a compressive pressure gradient, which is Darcy's Law. The third term can be recognised as the gradient of a chemical potential. The entropy gradient included in this term results in classical Fickian diffusion if only mixing entropy exists. For a detailed derivation and discussion of Equation (11), the reader is directed to Garikipati et al. (2004).

Since the driving forces in (11) originate from different physics, it proves useful (as seen in the following section) to rewrite (11) as

$$M^f = D_P^f F^T \text{DIV} [P^f] - D_\mu^f \text{GRAD} [e^f - \theta \eta^f], \quad (12)$$

where  $D_P^f$  is now the permeability of the tissue, corresponding to stress gradient-driven transport, and  $D_\mu^f$  is the mobility, corresponding to chemical potential gradient-driven transport, of the fluid phase through the porous solid.

### 3.3.1 Saturation and Fickian diffusion of the fluid

As depicted in Figure 6, only when pores are unsaturated are there multiple configurations available to the fluid molecules at a fixed fluid concentration. This leads to a non-zero mixing entropy. In contrast, if saturated, there is a single available configuration (degeneracy), resulting in zero mixing entropy. Consequently, Fickian diffusion, which arises from the gradient of mixing entropy can exist only in the unsaturated case. However, even a saturated pore structure can demonstrate concentration gradient-dependent mass transport phenomenologically: The fluid stress depends on fluid concentration, see Equation (9), and fluid stress gradient-driven flux appears as concentration gradient-driven flux.

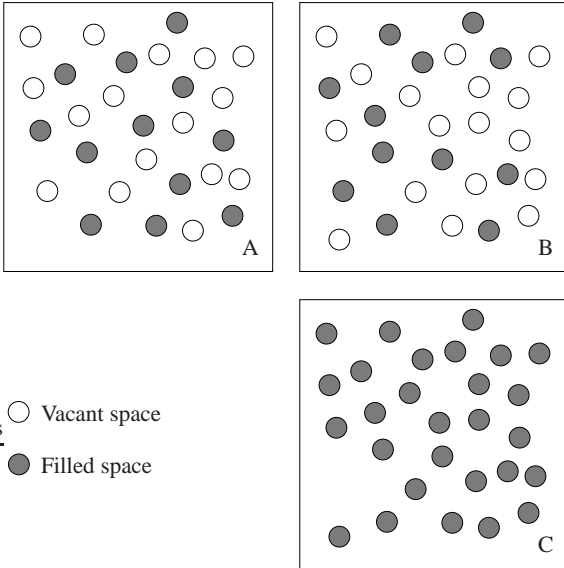


**Fig. 6** Depicted at a microscopic scale, only unsaturated tissues A and B can undergo Fickian diffusion of the fluid. C is saturated.

The saturation dependence of Fickian diffusion is modelled by using the measure of saturation introduced in Section 2.2.1. We first rewrite the chemical potential gradient term in (12) as

$$D_\mu^f \text{GRAD}[e^f - \theta\eta^f] = D_e^f \text{GRAD}[e^f] - D_\eta^f \text{GRAD}[\theta\eta^f], \quad (13)$$

where  $D_e^f$  and  $D_\eta^f$  are positive semi-definite mobilities, and the mobility for the Fickian contribution is

$$D_\eta^f = \begin{cases} \widetilde{D}_\eta^f, & \text{if } \sum_t \widetilde{v}^t < 1 \\ \mathbf{0}, & \text{otherwise.} \end{cases} \quad (14)$$

It is again important to note that under physiological conditions, soft tissues are fully saturated by fluid, and it is appropriate to set  $D_\eta^f = \mathbf{0}$ .

### 3.3.2 Transport of solute species

The numerous dissolved solute species (proteins, sugars, nutrients, ...), denoted by  $s$ , undergo long range transport primarily by being advected by the fluid. In addition to this, they undergo diffusive transport relative to the fluid. This motivates an additional velocity split of the form  $V^s = \widetilde{V}^s + V^f$ , where  $\widetilde{V}^s$  denotes the velocity of the solute relative to the fluid. The constitutive relation for the corresponding flux, denoted by  $\widetilde{M}^s$ , has the following form, similar to Equation (11) defined for the fluid flux.

$$\widetilde{M}^s = D^s (-\text{GRAD}[e^s - \theta\eta^s]), \quad (15)$$

where  $D^s$  is the positive semi-definite mobility of the solute relative to the fluid, and again, isothermal conditions are assumed to approximate the physiological ones. Being in solution, this phase does not bear appreciable stress, and the

stress divergence term is absent from the constitutive relation.

### 3.3.3 Frame invariance and the contribution from acceleration

In our earlier treatment (Garikipati et al., 2004), the constitutive relation for the fluid flux had a driving force contribution arising from the acceleration of the solid phase,  $-\rho_0^f F^T \frac{\partial V}{\partial t}$ . This term, being motivated by the reduced dissipation inequality, does not violate the Second Law and supports our intuitive understanding that accelerating the solid skeleton in one direction must result in an inertial driving force on the fluid in the opposite direction. However, as defined, this acceleration is obtained by the time differentiation of kinematic quantities,<sup>6</sup> and does not transform in a frame-indifferent manner. Unlike the superficially similar term arising from the gravity vector,<sup>7</sup> the acceleration term presents an improper dependence on the frame of the observer. Thus, its use in constitutive relations is inappropriate, and the term has been dropped in Equation (11).

### 3.3.4 Incompressible fluid in a porous solid

Upon incorporation of the additional velocity split,  $V^s = \widetilde{V}^s + V^f$ , described in Section 3.3.2, the resulting mass transport equation (3) for the solute species is

$$\frac{d\rho^s}{dt} = \pi^s - \text{div} \left[ \widetilde{m}^s + \frac{\rho^s}{\rho^f} m^f \right] - \rho^s \text{div}[v]. \quad (16)$$

In the hyperbolic limit, where advection dominates, spatial oscillations emerge in numerical solutions of this equation (Brooks and Hughes, 1982; Hughes et al., 1987). However, the form in which the equation is obtained is not in standard advection-diffusion form, and therefore is not amenable to the application of standard stabilisation techniques (Hughes et al., 1987). In part, this is because although the (near) incompressibility of the fluid phase is embedded in the balance of linear momentum via the fluid stress, it has not yet been explicitly incorporated into the transport equations. This section proceeds to impose the fluid incompressibility condition and deduces implications for the solute mass transport equation, including a crucial simplification allowing for its straightforward numerical stabilisation.

From Equation (3), the local form of the balance of mass for the fluid species (recalling that  $\Pi^f = 0$ ) in the current configuration is

$$\frac{d\rho^f}{dt} = -\text{div}[m^f] - \rho^f \text{div}[v]. \quad (17)$$

<sup>6</sup> And not in terms of acceleration *relative to fixed stars* for e.g., as discussed in Truesdell and Noll (1965).

<sup>7</sup> Where every observer has an implicit knowledge of the directionality of the field relative to a fixed frame, allowing it to transform objectively.

In order to impose the incompressibility of the fluid, we first denote by  $\rho_{0_{\text{ini}}}^f$  the *initial* value of the fluid reference concentration, and recognise that

$$\begin{aligned}\rho_0^f(X, 0) &=: \rho_{0_{\text{ini}}}^f(X) \\ &= \rho_{\text{ini}}^f(x \circ \varphi) J(X, t) \\ &= \frac{\rho^f(x \circ \varphi, t)}{J^{f_g}(X, t)} J(X, t) \\ &= \rho^f(x \circ \varphi, t) J^{f_g}(X, t).\end{aligned}\quad (18)$$

In (18),  $J$  denotes  $\det(F)$ ,  $J^{f_g}$  denotes  $\det(F^{g^f})$  and  $\rho_{\text{ini}}^f$  is the push-forward of  $\rho_{0_{\text{ini}}}^f$  to the current configuration.

Restricting the argument to a non-growing solid, i.e.  $F$  in the solid and  $F^{c_e}$  are identical,

$$\frac{\partial}{\partial t}(\rho_{0_{\text{ini}}}^f(X)) \equiv 0 \Rightarrow \frac{\partial}{\partial t}(\rho^f(x \circ \varphi, t))|_X = 0, \quad (19)$$

which is the hidden implication of our assumption of a homogeneous deformation, i.e.,  $F$  is the deformation gradient of all phases. This leads to  $\frac{d\rho^f}{dt} = 0$ .<sup>8</sup> We therefore proceed to treat our fluid mass transport at steady state. Rewriting the flux  $m^f$  from Equation (17) as the product  $\rho^f v^f$  and using the result derived above,

$$\begin{aligned}0 &= \frac{\partial \rho^f}{\partial t}|_X \\ &= -\text{div}[\rho^f v^f] - \rho^f \text{div}[v].\end{aligned}\quad (20)$$

Returning to (16) with this result,

$$\begin{aligned}\frac{d\rho^s}{dt} &= \pi^s - \text{div}\left[\widetilde{m}^s + \frac{\rho^s}{\rho^f} m^f\right] - \rho^s \text{div}[v] \\ &= \frac{\rho^s}{\rho^f} \left( -\text{div}[\rho^f v^f] - \rho^f \text{div}[v] \right) \\ &\quad + \pi^s - \text{div}[\widetilde{m}^s] - m^f \cdot \text{grad}\left[\frac{\rho^s}{\rho^f}\right].\end{aligned}\quad (21)$$

Thus, using the incompressibility condition (20), we get the simplified form of the balance of mass for an arbitrary solute species,  $s$ ,

$$\frac{d\rho^s}{dt} = \pi^s - \text{div}[\widetilde{m}^s] - \frac{m^f \cdot \text{grad}[\rho^s]}{\rho^f} + \frac{\rho^s m^f \cdot \text{grad}[\rho^f]}{\rho^f}. \quad (22)$$

Using the pushed-forward form of (15), this is now in standard advection-diffusion form,

$$\begin{aligned}\frac{d\rho^s}{dt} - \underbrace{\text{div}[\bar{D}^s \text{grad}[\rho^s]]}_{\text{Diffusion term}} - \underbrace{\pi^s}_{\text{Source term}} &= \\ - \underbrace{\frac{m^f \cdot \text{grad}[\rho^s]}{\rho^f}}_{\text{Advection term}} + \underbrace{\frac{\rho^s m^f \cdot \text{grad}[\rho^f]}{\rho^f^2}}_{\text{Additional, } \rho^s\text{-dependent source term}},\end{aligned}\quad (23)$$

where  $\bar{D}^s$  is a positive semi-definite diffusivity,  $m^f/\rho^f$  is the advective velocity, and  $\pi^s$  is the volumetric source term. This form is well suited for stabilisation schemes such as the streamline upwind Petrov-Galerkin (SUPG) method (see, for e.g., Hughes et al. (1987)), described briefly below, which limit spatial oscillations otherwise observed when the element *Peclet number* is large.

### 3.3.5 Stabilisation of the simplified solute transport equation

In weak form, the SUPG-stabilised method for Equation (23) is

$$\begin{aligned}\int_{\Omega} w^h \left( \frac{d\rho^{s^h}}{dt} + m^f \cdot \text{grad} \left[ \frac{\rho^{s^h}}{\rho^f} \right] \right) d\Omega \\ + \int_{\Omega} \left( \text{grad}[w^h] \cdot \bar{D}^s \text{grad}[\rho^{s^h}] \right) d\Omega \\ + \sum_{e=1}^{n_{\text{el}}} \int_{\Omega_e} \tau \frac{m^f}{\rho^f} \cdot \text{grad}[w^h] \left( \frac{d\rho^{s^h}}{dt} + m^f \cdot \text{grad} \left[ \frac{\rho^{s^h}}{\rho^f} \right] \right) d\Omega \\ - \sum_{e=1}^{n_{\text{el}}} \int_{\Omega_e} \tau \frac{m^f}{\rho^f} \cdot \text{grad}[w^h] \left( \text{div}[\bar{D}^s \text{grad}[\rho^{s^h}]] \right) d\Omega \\ = \int_{\Omega} w^h \pi^s d\Omega + \int_{\Gamma_h} w^h h d\Gamma \\ + \sum_{e=1}^{n_{\text{el}}} \int_{\Omega_e} \tau \frac{m^f}{\rho^f} \cdot \text{grad}[w^h] \pi^s d\Omega,\end{aligned}\quad (24)$$

where quantities with the superscript  $h$  represent finite-dimensional approximations of infinite-dimensional field variables,  $\Gamma_h$  is the Neumann boundary, and this equation introduces a numerical stabilisation parameter  $\tau$ , which we have calculated from the  $L_2$  norms of element level matrices, as described in Tezduyar and Sathe (2003).

### 3.4 Nature of the sources

There exists a large body of literature, Cowin and Hegedus (1976); Epstein and Maugin (2000); Ambrosi and Mollica (2002), that addresses growth in biological tissue mainly based upon a single species undergoing transport and production/annihilation. However, when chemistry is accounted for, it is apparent

<sup>8</sup> Which results in a very large pressure gradient driven flux due to incompressibility.

that growth depends on cascades of complex biochemical reactions involving several species, and additionally involves intimate coupling between mass transfer, biochemistry and mechanics. An example of this chemo-mechanical coupling is described in Provenzano et al. (2003).

The modelling approach followed in this work is to select appropriate functional forms of the source terms for collagen,  $\Pi^c$ , and the solutes,  $\Pi^s$ , that abstract the complexity of the biochemistry. In our earlier exposition (Garikipati et al., 2004), we utilised simple first order chemical kinetics to define  $\Pi^c$ . Our current models now replace it with two sources that have greater relevance from the standpoint of biochemistry.

The first of these is *Michaelis-Menten* enzyme kinetics (see, for e.g., Sengers et al. (2004)), which involves a two-step reaction with the collagen and solute production terms given by

$$\Pi^s = \frac{-(k_{\max}\rho^s)}{(\rho_m^s + \rho^s)}\rho_{\text{cell}}, \quad \Pi^c = -\Pi^s, \quad (25)$$

where  $\rho_{\text{cell}}$  is the concentration of fibroblasts,  $k_{\max}$  is the maximum value of the solute production reaction rate constant, and  $\rho_m^s$  is half the solute concentration corresponding to  $k_{\max}$ . For details on the chemistry modelled by the Michaelis-Menten model, see, for e.g., Bromberg and Dill (2002).

The second is a *strain-energy dependent* source term that was originally proposed in the context of bone growth (Harrigan and Hamilton 1993), and induces growth at a point when the energy density deviates from a basal value, suitably weighted by a relative density ratio. Written for collagen, it has the form

$$\Pi^c = \left( \frac{\rho_0^c}{\rho_{0,\text{ini}}^c} \right)^{-m} \psi_F - \psi_F^*, \quad (26)$$

where  $\psi_F$  is the mass-specific strain energy function, and  $\psi_F^*$  is a reference value of this strain energy density. Equation (26) models collagen production when the strain energy density (weighted by a relative density ratio) at a point exceeds this reference value, and models annihilation otherwise.

#### 4 Numerical examples

The theory presented in the preceding sections results in a system of non-linear coupled partial differential equations. A finite element formulation employing a staggered scheme based upon operator splits Armero (1999); Garikipati and Rao (2001) has been implemented in FEAP (Taylor, 1999) to solve the coupled problem. For example, in the biphasic problem involving a solid phase and a fluid phase, the basic solution scheme involves keeping the displacement field fixed while solving for the concentration fields using the mass transport equations. The resulting concentration fields are then fixed to solve the mechanics problem. This procedure is repeated until the resulting fields satisfy the differential equations within some error norm.

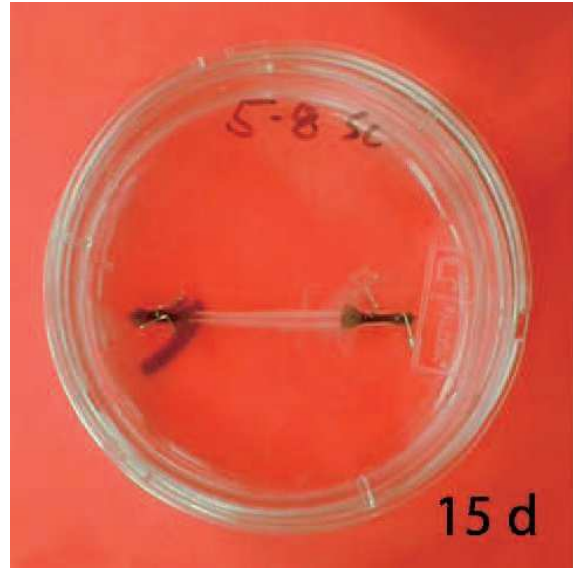


**Fig. 7** Engineered tendon constructs. See Calve et al. (2004) for details.

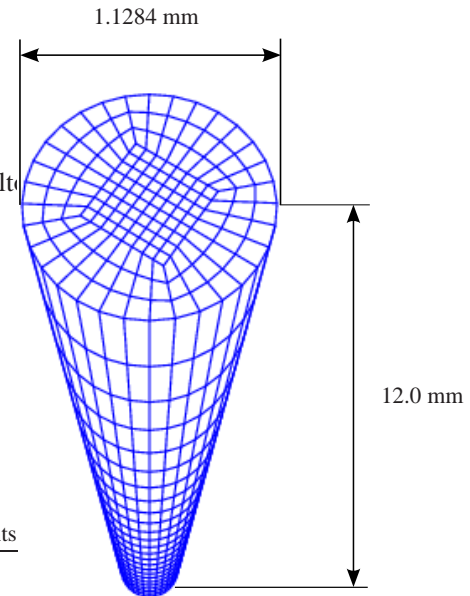


**Fig. 8** The finite element mesh used in the computations.

The following examples aim to demonstrate the mathematical formulation and aspects of the coupled phenomena as the tissue grows. The model geometry, based on our engineered tendon constructs (see Figure 7), is a cylinder 12 mm in length and 1 mm<sup>2</sup> in cross-sectional area. The corresponding finite element mesh used in the computations, using hexahedral elements, is shown in Figure 8.

The absence of significant acceleration in the problems under consideration prompts us to solve the balance of linear momentum quasi-statically. Backward Euler is used as the time-stepping algorithm for mass transport. Non-linear projection methods (Simo et al., 1985) are used to treat the

Parameter (Symbol)	Value	Units
Chain density ( $N$ )	$7 \times 10^{21}$	$\text{m}^{-3}$
Temperature ( $\theta$ )	310.6	K
Persistence length ( $A$ )	2.10	—
Fully-stretched length ( $L$ )	2.125	—
Unit cell axes ( $a, b, c$ )	1.95, 1.95, 2.43	—
Bulk compressibility factors ( $\gamma, \beta$ )	1000, 4.5	—
Fluid bulk modulus ( $k^f$ )	1	GPa
Fluid mobility tensor ( $D_{ij} = D\delta_{ij}$ )	$1 \times 10^{-14}$	s
Fluid mol. wt. ( $\mathcal{M}^f$ )	$2.991 \times 10^{-26}$	kg

**Table 1** Material parameters used in the analysis.

near-incompressibility imposed by water. Mixed methods, as described in Garikipati and Rao (2001), are used for stress (and strain) gradient driven fluxes.

#### 4.1 Examples using first order chemical kinetics

In these calculations, only two phases—fluid and collagen—are included for the mass transport and mechanics. The collagen phase,  $c$ , is modelled by the anisotropic worm-like chain model outlined previously (see Section 3.1) and the fluid phase is modelled as ideal and nearly incompressible. The parameters used in the analysis are presented in Table 1 and the values chosen are representative of tendons. The classes of initial and boundary conditions imposed are based on experiments in our laboratory.

In order to demonstrate growth with only two species, an “artificial” fluid sink  $\Pi^f$  is introduced following simple first order kinetics,

$$\Pi^f = -k^f(\rho_0^f - \rho_{0\text{ini}}^f), \quad (27)$$

as in Garikipati et al. (2004). Here  $k^f$  is the reaction rate (taken to be  $0.07 \text{ s}^{-1}$  in the following examples) and  $\rho_{0\text{ini}}^f$  is the initial concentration of fluid. The collagen source will be the negative of the fluid sink:  $\Pi^c = -\Pi^f$ . When  $\rho_0^f > \rho_{0\text{ini}}^f$ , this acts as a source for collagen. The mixing entropy of fluid in the mixture with collagen is written as  $\eta_{\text{mix}}^f = -\frac{k}{\mathcal{M}^f} \log(\frac{\rho^f}{\rho})$ , where  $\mathcal{M}^f$  is the molecular weight of the fluid.

##### 4.1.1 A swelling problem

The boundary conditions in this example correspond to immersion of the tendon in a nutrient-rich bath. The initial collagen concentration is  $500 \text{ kg.m}^{-3}$  and the fluid concentration is  $400 \text{ kg.m}^{-3}$  at every point in the tendon. When this tendon is exposed to a bath where the fluid concentration is  $410 \text{ kg.m}^{-3}$ , i.e.  $\rho^f(x, t) = 410 \text{ kg.m}^{-3} \forall x \in \partial\Omega_t$ , nutrient-rich fluid is transported into the tissue, and growth occurs due to the formation of additional collagen.

Figure 9 shows the initial collagen concentration in the tendon. After it has been immersed in the nutrient-rich bath for 1800 s, the tendon shows growth and the collagen concentration is higher as seen in Figure 10. On performing a simple uniaxial tension test on the tendon before and after



**Fig. 9** The collagen initial concentration ( $\text{kg.m}^{-3}$ ).

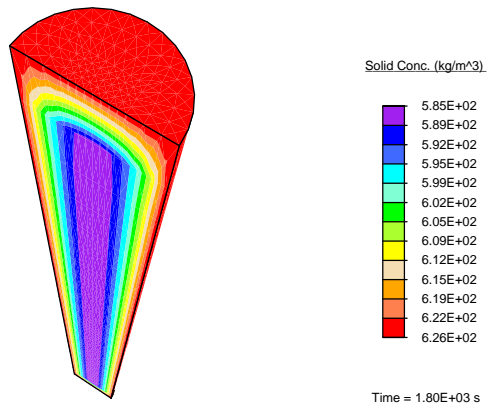


**Fig. 10** The collagen concentration ( $\text{kg.m}^{-3}$ ) after 1800 s.

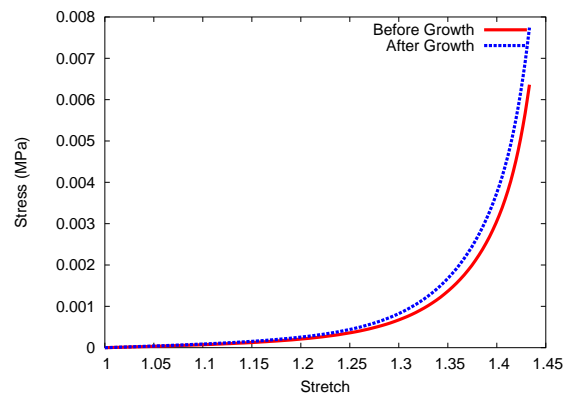


**Fig. 11** The stress (Pa) vs stretch curves before and after growth.

growth, it is observed that the grown tissue is stiffer and stronger as seen in Figure 11, which is in accordance with experiment. In addition, there is a rapid, fluid transport-dominated swelling of the tendon initially (Figure 12) as it is immersed in the fluid bath. A reaction-driven growth phase then follows, but its rate is too small to demonstrate significant growth over the time scale of the computation. For this

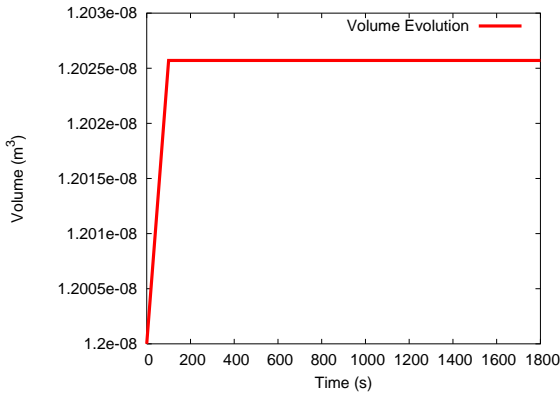


**Fig. 12** The volume of the tendon ( $\text{m}^3$ ) evolving with time.

reason Figure 12 appears to have a vanishing growth rate beyond  $t \approx 80$  s.

#### 4.1.2 The tendon under constriction

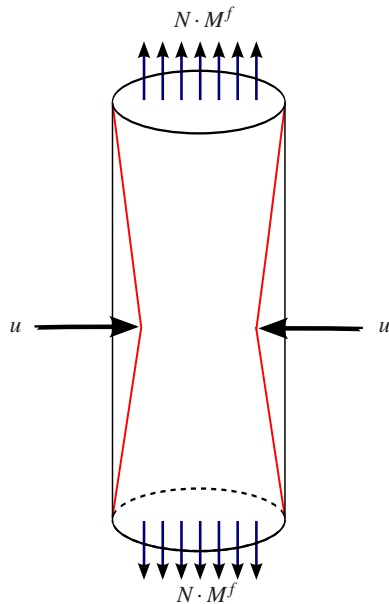


**Fig. 13** Constrictive load applied to tendon immersed in a bath.

In this example, the tendon immersed in a bath is subjected to a constrictive radial load as depicted in Figure 13. The maximum strain in the radial direction—experienced half-way through the height of the tendon—is 10%. The applied strain in the radial direction decreases linearly with distance from the central plane, and vanishes at the top and bottom surfaces of the tendon. The total duration of the simulation is 10 s, and the radial strain is applied as a displacement boundary condition, increasing linearly from no strain initially to the maximum strain at time  $t = 1$  s.

Since an insignificant amount of local collagen production/fluid conversion takes place over this time scale, we

have simplified the problem by setting the source terms  $\Pi^c = 0$  and  $\Pi^f = 0$ . In this case, both the initial collagen concentration and the initial fluid concentration are  $500 \text{ kg.m}^{-3}$  at every point in the tendon. This tendon is exposed to a bath where the fluid concentration is  $500 \text{ kg.m}^{-3}$ .

While solving the balance of momentum for the biphasic problem involving a solid phase and a fluid phase, we currently treat the tissue as a single entity and employ a summation of Equation (6) over both species. Additionally, condition (7) allows us to avoid constitutive prescription of the momentum transfer terms between species,  $q^t$ . This facilitates considerable simplification of the problem, but such a treatment requires additional assumptions on the detailed deformation of the constitutive phases of the tissue. An implicit assumption we have drawn on thus far is the equality of the deformation gradient of the solid collagen and fluid phases,  $F = F^c = F^f$ . Recognising that such an ansatz plays a fundamental role in determining the fluid flux (driven by the pressure gradient), and, furthermore, that such an assumption of common deformation gradient results in an upper bound for the effective stiffness of the tissue and magnitudes of the fluxes established, we refer to it as the *upper bound model*.

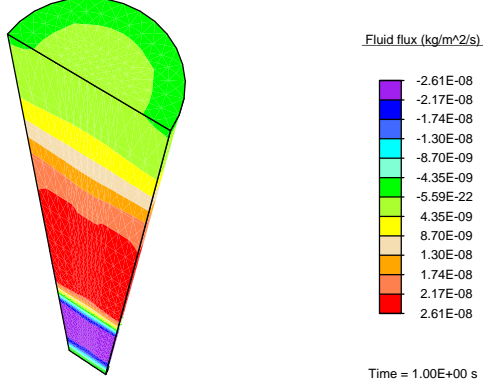


**Fig. 14** Upper bound fluid flux ( $\text{kg.m}^{-2}.\text{s}^{-1}$ ) in the vertical direction at time  $t = 1$  s.

For this model, Figure 14 shows the fluid flux in the vertical direction at the final stage of the constriction phase of the simulation, i.e. at time  $t = 1$  s. The flux values are positive above the central plane, forcing fluid upward, and negative below, forcing fluid downward. This stress-gradient induced fluid flux results in a reference concentration distribution of the fluid that is higher near the top and bottom faces, as seen in Figure 15.

As a result, these regions would have seen a higher production of collagen, or preferential growth, in the presence of non-zero source terms. As discussed in Section 2.1.1, the mass transport equations are solved in the current configuration, where physical boundary conditions can be set directly. The values reported in Figure 15 are pulled back from the current configuration. The current concentrations do not

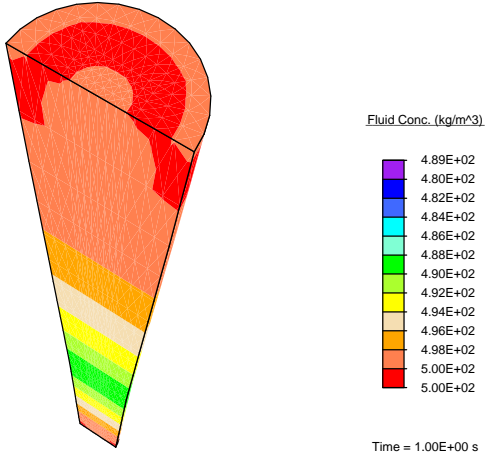


Fig. 15 Reference fluid concentration ( $\text{kg.m}^{-3}$ ) at time  $t = 1$  s.

change for this boundary value problem. Solving a problem of this nature in the reference configuration using a similar constant concentration boundary to represent immersion of the tendon in a fluid bath yields non-physical results, such as an unbounded flow. This occurs since the imposed strain gradient causes a stress gradient in the fluid that does not decay. The imposed boundary condition on  $\rho_0$  prevents a redistribution of concentration that would have provided an opposing, internal gradient of stress, which in turn would drive the flux to vanish.

The tendon is held fixed in the radial direction after the constriction phase. The applied stress sets up a pressure wave in the fluid travelling toward the top and bottom faces. As the fluid leaves these surfaces, we observe that the tendon relaxes. This is seen in Figure 16, which plots the vertical displacement of the top face with time, showing a decrease in height of the tendon after the constriction phase. We keep the centre of the bottom face of the tendon fixed.

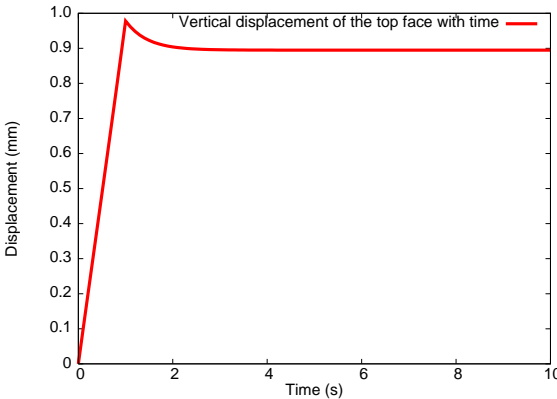


Fig. 16 Relaxation of the top face of the tendon after the constriction phase.

In order to define a range of the magnitude of fluid flux, we now introduce the *lower bound model* (on effective stiffness of the tissue and, consequently, the magnitude of the fluid flux). For this lower bound, we replace the earlier strain homogenisation requirement with a stress homogenisation requirement, *viz.* equating the hydrostatic stress of the solid phase and the fluid pressure in the current configuration:

$$p^f = \frac{1}{3} \text{tr}[\sigma^c], \quad (28)$$

where  $p^f$  is the fluid pressure in the current configuration,  $\text{tr}[\bullet]$  is the trace operator, and  $\sigma^c = \frac{1}{J^c} P^c F^{cT}$  is the Cauchy stress of the solid. The Cauchy stress of an ideal fluid can be defined from its current pressure as  $\sigma^f = p^f \mathbf{1}$ . Figure 17 reports the value of the vertical flux under the lower bound modelling assumption, using boundary conditions identical to the previous calculation at time  $t = 1$  s, the final stage of the constriction phase of the simulation.

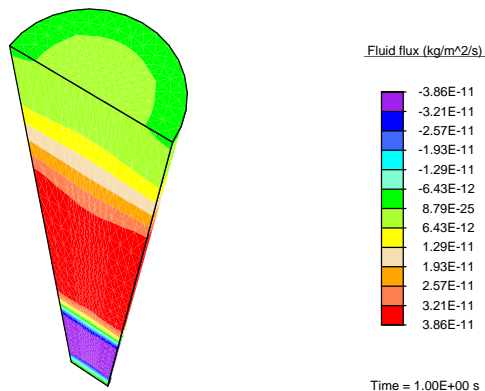


Fig. 17 Lower bound fluid flux ( $\text{kg.m}^{-2}.\text{s}^{-1}$ ) in the vertical direction at time  $t = 1$  s.

The fluid flux values reported in Figures 14 and 17 (corresponding to the upper and lower bound modelling assumptions, respectively) are qualitatively similar, but differ by about three orders of magnitude. These results bracket the range of possible fluid flux values under the specified mechanical loading. In future work, we will detail a more comprehensive treatment of the momentum equations, resulting in better estimation of the fluxes.

Furthermore, we recognise that a convenient measure of the strength of coupling between the mechanics and mass transport equations is the ratio of the variation in hydrostatic stress of the fluid to that of the solid. In the lower bound case, where the fluid response is defined by Equation (28), it is instructive to note that this ratio is unity. As a result, it is seen that the lower bound case exhibits significantly weaker coupling than the upper bound case. In the latter, variation in the common deformation gradient,  $\delta F$ , causes instantaneous variation in  $p^f \approx O(\kappa^f \delta F : F^{-T})$  and in

$\frac{1}{3}\text{tr}[\sigma^c] \approx O(\kappa^c \delta F : F^{-T})$ , where  $\kappa^c$  is the bulk modulus of the solid. The ratio  $\frac{\delta p^f}{\frac{1}{3}\delta\text{tr}[\sigma^c]}$  is therefore  $\approx O(\kappa^f/\kappa^c) \gg 1$ .

The strength of coupling between the equations plays a principal role in the rate of convergence of the solution, as observed in Table 2, where the mechanics equation residual norms (and corresponding CPU times in seconds for an Intel®Xeon 3.4 GHz machine) are reported for the first 8 iterations of each of the two cases. The staggered scheme involves solution of the mechanics equation keeping the concentrations fixed, and the mass transport equation keeping the displacements fixed, in turn, until the solution converges. The table does not report the value of the residual norms arising from the solution of the mass transport equation for the fluid, which occurs after each reported solve of the mechanics equation. Though the initial mechanics residual norms in subsequent passes are decreasing linearly in both cases, the rapid drop in the weakly-coupled case ensures convergence in far fewer iterations than the strongly coupled case. Thus, the corresponding CPU times reported are also lower for the weakly coupled case. This is advantageous, as in addition to being closer to physiological reality, the lower bound, weakly-coupled case makes it feasible to drive problems to longer, physiologically-relevant time-scales through the use of larger time steps.

#### 4.2 A multiphasic problem based on enzyme-kinetics

This final example can be viewed as a model for localised, bolus delivery of regulatory chemicals to the tendon while accounting for mechanical (stress) effects. It is substantially more complex than the previous cases, and involves additional species (a solute<sup>9</sup> denoted by  $s$ , and a uniform distribution of fibroblasts that are characterised by their cell concentration,  $\rho_{\text{cell}}$ ). Both the concentration gradient driven mass transport seen in Example 4.1.1 as well as the stress gradient driven fluid flow seen in Example 4.1.2 are incorporated in this illustration. We use Michaelis-Menten enzyme kinetics [Equation (25)] to determine the rates of solute consumption and collagen production as a function of solute concentration. This non-linear relationship for our choice of parameters is visualised in Figure 18. Here, the fluid phase does not take part in reactions, and hence  $\Pi^f = 0$ .

The tendon immersed in the bath is subjected to the constrictive radial load discussed in the Example 4.1.2. As before, the initial collagen concentration and the initial fluid concentration are both  $500 \text{ kg.m}^{-3}$  at every point in the tendon, and the fluid concentration in the bath is  $500 \text{ kg.m}^{-3}$ . In addition, a solute-rich bulb of radius 0.15 mm is introduced with its centre on the axis of the tendon and situated 3 mm below the top face of the tendon. The initial solute

<sup>9</sup> Here, we envision the solute to be a protein playing an essential role in growth by catalysing underlying biochemical reactions. An important example of this is a family of proteins, TGF $\beta$ , which is a multifunctional peptide that controls numerous functions of many cell types (Alberts et al., 2002).

Pass	Strongly coupled		Weakly coupled	
	Residual	CPU (s)	Residual	CPU (s)
1	$2.138 \times 10^{-02}$	29.16	$6.761 \times 10^{-04}$	28.5
	$3.093 \times 10^{-04}$	55.85	$1.075 \times 10^{-04}$	55.1
	$2.443 \times 10^{-06}$	82.37	$4.984 \times 10^{-06}$	81.8
	$2.456 \times 10^{-08}$	109.61	$1.698 \times 10^{-08}$	107.9
	$4.697 \times 10^{-14}$	135.83	$3.401 \times 10^{-13}$	134.1
	$1.750 \times 10^{-16}$	163.18	$1.1523 \times 10^{-17}$	161.1
2	$5.308 \times 10^{-06}$	166.79	$5.971 \times 10^{-08}$	192.5
	$4.038 \times 10^{-10}$	193.36	$4.285 \times 10^{-11}$	218.6
	$1.440 \times 10^{-14}$	220.45	$2.673 \times 10^{-15}$	246.1
	$4.221 \times 10^{-17}$	247.04		
3	$5.186 \times 10^{-06}$	250.62	$2.194 \times 10^{-09}$	277.3
	$3.852 \times 10^{-10}$	277.44	$2.196 \times 10^{-13}$	304.2
	$1.369 \times 10^{-14}$	304.16	$1.096 \times 10^{-17}$	331.6
	$4.120 \times 10^{-17}$	331.47		
4	$5.065 \times 10^{-06}$	335.16	$8.160 \times 10^{-11}$	363.2
	$3.674 \times 10^{-10}$	362.24	$7.923 \times 10^{-15}$	390.2
	$1.300 \times 10^{-14}$	388.79		
	$4.021 \times 10^{-17}$	416.08		
5	$4.948 \times 10^{-06}$	419.59	$3.078 \times 10^{-12}$	421.4
	$3.503 \times 10^{-10}$	446.24	$3.042 \times 10^{-16}$	448.6
	$1.236 \times 10^{-14}$	473.20		
	$3.924 \times 10^{-17}$	500.85		
6	$4.832 \times 10^{-06}$	504.65	$1.179 \times 10^{-13}$	479.9
	$3.340 \times 10^{-10}$	531.28	$1.291 \times 10^{-17}$	507.0
	$1.174 \times 10^{-14}$	558.17		
	$3.829 \times 10^{-17}$	585.27		
7	$4.720 \times 10^{-06}$	589.01	$4.592 \times 10^{-15}$	537.8
	$3.184 \times 10^{-10}$	616.24	$5.152 \times 10^{-18}$	564.6
	$1.116 \times 10^{-14}$	643.29		
	$3.737 \times 10^{-17}$	670.83		
8	$4.609 \times 10^{-06}$	674.46	$1.816 \times 10^{-16}$	595.5
	$3.034 \times 10^{-10}$	701.74	$5.040 \times 10^{-18}$	622.3
	$1.060 \times 10^{-14}$	727.74		
	$3.646 \times 10^{-17}$	755.58		

**Table 2** Mechanics equation residual norms and corresponding CPU times in seconds for the first 8 passes of each of the two cases for a typical time increment,  $\Delta t = 0.1$  s.

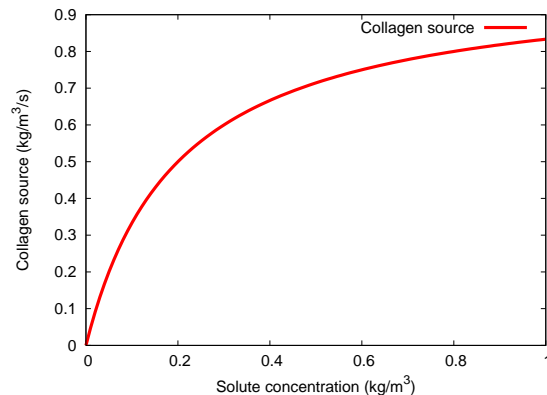


**Fig. 18** Variation of the collagen source term ( $\text{kg.m}^{-3} \cdot \text{s}^{-1}$ ) with solute concentration ( $\text{kg.m}^{-3}$ ).

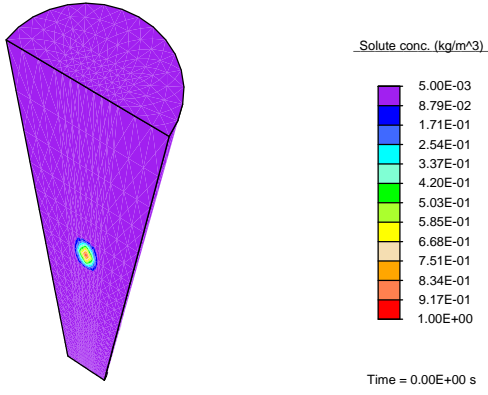


**Fig. 19** The solute concentration ( $\text{kg.m}^{-3}$ ) initially.

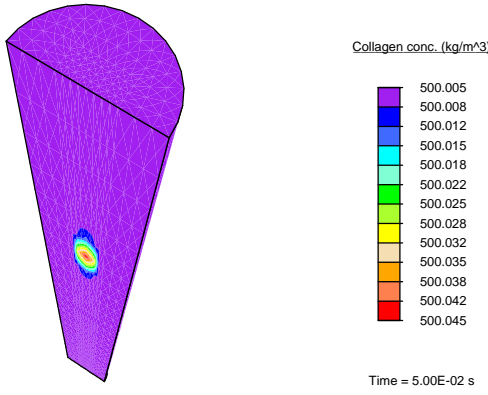


**Fig. 20** The collagen concentration ( $\text{kg.m}^{-3}$ ) at time  $t = 5 \times 10^{-2}$  s.

concentration is  $0.05 \text{ kg.m}^{-3}$  at all other points in the tendon, and increases linearly with decreasing radius in this bulb to  $1 \text{ kg.m}^{-3}$  at its centre (see Figure 19). Augmenting the parameters listed in Table 1, this calculation uses the following parameters:  $\rho_{\text{cell}} = 0.2 \text{ kg.m}^{-3}$ ,  $k_{\text{max}} = 5 \text{ s}^{-1}$ ,  $\rho_m^s = 0.2 \text{ kg.m}^{-3}$ ,  $D^s = 1 \times 10^{-9} \text{ m}^2 \text{s}^{-1}$ .

This calculation uses the upper bound model for fluid flow, but because the magnitude of the fluid mobility is orders of magnitude smaller than the diffusion coefficient for the solute through the fluid, there is relatively only a small stress gradient driven flux, and the transport of the solute is diffusion dominated. As a result, as time progresses, the solute diffuses locally and as the solute concentration in a region increases, the enzyme-kinetics model predicts a small source term for collagen, and we observe nominal growth. Figure 20 shows the collagen concentration at an early time,  $t = 5 \times 10^{-2}$  s.

Though this example incorporates much of the theory discussed in this paper, modelling choices made for this example and the associated selection of parameters, as well as the initial and boundary conditions used, are primarily chosen to demonstrate the applicability of the theory. The specifics of these modelling choices for this specific problem remain open questions, and we need to investigate combina-

tions of different driving forces (mechanics, chemical potential gradients, body forces), as well as appropriate choices for the sources, for accurate modelling of the chemomechanics of growth.

## 5 Conclusion

In this paper, we have discussed a number of enhancements to our original growth formulation presented in Garikipati et al. (2004). That formulation has served as a platform for posing a very wide range of questions on the biophysics of growth. Some issues, such as saturation, incompressibility of the fluid species and its influence upon the tissue response, and the roles of biochemical and strain energy-dependent source terms are specific to soft biological tissues. We note, however, that other issues are also applicable to a number of systems with a porous solid, transported fluid and reacting solutes. Included in these are issues of current versus reference configurations for mass transport, swelling, Fickian diffusion, fluid response in compression and tension, cavitation, and roles of permeabilities and mobilities.

These issues have been resolved using arguments posed easily in the framework derived in Garikipati et al. (2004). The interactions engendered in the coupled reaction-transport-mechanics system are complex, as borne out by the numerical examples in Section 4. We are currently examining combinations of sources defined in Section 3.4, and aim to calibrate our choices from tendon growth experiments. The treatment of these issues has led to a formulation more suited to the biophysics of growing soft tissue, making progress toward our broader goal of applying it to the study of wound healing, pathological hypertrophy and atrophy, as well as a study of drug efficacy and interaction.

## References

- Alberts B, Johnson A, Lewis J, Raff M, Roberts K, Walter P (2002) *Molecular Biology of the Cell*. Garland Science, Oxford
- Ambrosi D, Mollica F (2002) On the mechanics of a growing tumor. *Int J Engr Sci* 40:1297–1316
- Armero F (1999) Formulation and finite element implementation of a multiplicative model of coupled poroplasticity at finite strains under fully-saturated conditions. *Comp Methods in Applied Mech Engrg* 171:205–241
- Bischoff JE, Arruda EM, Grosh K (2002a) A microstructurally based orthotropic hyperelastic constitutive law. *J Applied Mechanics* 69:570–579
- Bischoff JE, Arruda EM, Grosh K (2002b) Orthotropic elasticity in terms of an arbitrary molecular chain model. *J Applied Mechanics* 69:198–201
- Brennen CE (1995) *Cavitation and Bubble Dynamics*. Oxford University Press

Bromberg S, Dill KA (2002) Molecular Driving Forces: Statistical Thermodynamics in Chemistry and Biology. Garland

Brooks A, Hughes T (1982) Streamline upwind/Petrov-Galerkin formulations for convection dominated flows with particular emphasis on the incompressible Navier-Stokes equations. *Comp Methods in Applied Mech Engrg* 32:199–259

Bustamante C, Bryant Z, Smith SB (2003) Ten years of tension: Single-molecule DNA mechanics. *Nature* 421:423–427

Calve S, Dennis R, Kosnik P, Baar K, Grosh K, Arruda E (2004) Engineering of functional tendon. *Tissue Engineering* 10:755–761

Cowin SC, Hegedus DH (1976) Bone remodeling I: A theory of adaptive elasticity. *Journal of Elasticity* 6:313–325

Epstein M, Maugin GA (2000) Thermomechanics of volumetric growth in uniform bodies. *International Journal of Plasticity* 16:951–978

Fung YC (1993) Biomechanics: Mechanical properties of living tissues, 2nd edn. Springer-Verlag, New York

Garikipati K, Rao VS (2001) Recent advances in models for thermal oxidation of silicon. *Journal of Computational Physics* 174:138–170

Garikipati K, Arruda EM, Grosh K, Narayanan H, Calve S (2004) A continuum treatment of growth in biological tissue: Mass transport coupled with mechanics. *Journal of Mechanics and Physics of Solids* 52:1595–1625

Han S, Gemmell SJ, Helmer KG, Grigg P, Wellen JW, Hoffman AH, Sotak CH (2000) Changes in ADC caused by tensile loading of rabbit achilles tendon: Evidence for water transport. *Journal of Magnetic Resonance* 144:217–227

Harrigan TP, Hamilton JJ (1993) Finite element simulation of adaptive bone remodelling: A stability criterion and a time stepping method. *Int J Numer Methods Engrg* 36:837–854

Hughes T, Franca L, Mallet M (1987) A new finite element formulation for computational fluid dynamics: VII. Convergence analysis of the generalized SUPG formulation for linear time-dependent multidimensional advective-diffusive systems. *Comp Methods in Applied Mech Engrg* 63(1):97–112

Kratky O, Porod G (1949) Röntgenuntersuchungen gelöster Fadenmoleküle. *Recueil Trav Chim* 68:1106–1122

Kuhl E, Steinmann P (2003) Theory and numerics of geometrically-nonlinear open system mechanics. *Int J Numer Methods Engrg* 58:1593–1615

Kuhl E, Garikipati K, Arruda E, Grosh K (2005) Remodeling of biological tissue: Mechanically induced reorientation of a transversely isotropic chain network. *Journal of the Mechanics and Physics of Solids* 53(7):1552 – 73

Landau LD, Lifshitz EM (1951) A Course on Theoretical Physics, Volume 5, Statistical Physics, Part I. Butterworth Heinemann (reprint)

Lee EH (1969) Elastic-Plastic Deformation at Finite Strains. *J Applied Mechanics* 36:1–6

Marko JF, Siggia ED (1995) Stretching DNA. *Macromolecules* 28:8759–8770

Nordin M, Lorenz T, Campello M (2001) Biomechanics of tendons and ligaments. In: Nordin M, Frankel VH (eds) *Basic Biomechanics of the Musculoskeletal System*, Lippincott Williams and Wilkins, N.Y., pp 102–125

Provenzano PP, Martinez DA, Grindeland RE, Dwyver KW, Turner J, Vailas AC, Vanderby R (2003) Hindlimb unloading alters ligament healing. *Journal of Applied Physiology* 94:314–324

Rief M, Oesterhelt F, Heymann B, Gaub HE (1997) Single Molecule Force Spectroscopy o Polysaccharides by Atomic Force Microscopy. *Science* 275:1295–1297

Sengers BG, Oomens CWJ, Baaijens FPT (2004) An integrated finite-element approach to mechanics, transport and biosynthesis in tissue engineering. *J Bio Mech Engrg* 126:82–91

Simo JC, Taylor RL, Pister KS (1985) Variational and projection methods for the volume constraint in finite deformation elasto-plasticity. *Comp Methods in Applied Mech Engrg* 51:177–208

Sun YL, Luo ZP, Fertala A, An KN (2002) Direct quantification of the flexibility of type I collagen monomer. *Biochemical and Biophysical Research Communications* 295:382–386

Swartz M, Kaipainen A, Netti PE, Brekken C, Boucher Y, Grodzinsky AJ, Jain RK (1999) Mechanics of interstitial-lymphatic fluid transport: Theoretical foundation and experimental validation. *J Bio Mech* 32:1297–1307

Taber LA, Humphrey JD (2001) Stress-modulated growth, residual stress and vascular heterogeneity. *J Bio Mech Engrg* 123:528–535

Taylor RL (1999) FEAP - A Finite Element Analysis Program. University of California at Berkeley, Berkeley, CA

Tezduyar T, Sathe S (2003) Stabilization parameters in SUPG and PSPG formulations. *Journal of Computational and Applied Mechanics* 4:71–88

Truesdell C, Noll W (1965) The Non-linear Field Theories (Handbuch der Physik, band III). Springer, Berlin